A Cs Rydberg Atomic Microwave Oscillator for Electric Field Sensing

He Wang, David Rosser, Michael J. Mazon, and Gabe H. Iyanu
Electronics and Photonics Laboratory
The Aerospace Corporation, El Segundo, CA 90245 USA
he.wang@aero.org

Abstract **In this paper, we report an atomic oscillator in Ku band and its application for electric field (E-field) sensing with Cs Rydberg atoms in a room-temperature vapor cell. The oscillator is associated with the Cs Rydberg transition of $36^2D_{5/2} - 37^2P_{3/2}$ at 16.316 GHz which is generated with a two-laser double-resonance excitation. We characterized the energetics and the dipole moment of the Rydberg transition and used Electromagnetically Induced Transparency (EIT) and Autler-Townes (AT) effects for detecting continuous and amplitude/frequency modulated microwave E-fields. To enhance the oscillator's response to weak signals, a superheterodyne technique was incorporated into the Rydberg oscillator system, which resulted in an improvement in the oscillator's sensitivity by 100 times. Furthermore, our modeling shows that the Cs Rydberg atomic oscillator can be tuned to broad frequency ranges from MHz to THz for various RF applications.**

Keywords—Rydberg atoms, electric-field sensing, atomic oscillators.

I. INTRODUCTION

A Rydberg atomic system has quantum transitions falling into broad microwave frequency ranges from MHz to THz, covering from below L band all the way to mm waves [1-2]. Applications of Rydberg atomic oscillators include novel quantum sensors for self-calibrated electrometry and RF receivers and antennas [2-9]. In this paper, we present the experiment and characterization of a Cs Rydberg atomic microwave oscillator in Ku band at 16.316 GHz for continuous and time varying E-field sensing. The demonstrated Rydberg oscillator can be readily tuned to other microwave frequencies including VHF, UHF and L bands. Our work is aimed at investigating and mitigating the engineering and atomic physics limitations to the devices' size, weight, power, portability and reliability.

II. CS RYDBERG ATOMIC OSCILLATORS

Fig. 1 shows the atomic transition scheme for the Cs Rydberg microwave oscillator. A near-infrared laser, the probe laser at 852.4 nm, is used to induce a Doppler broadened absorption of Cs D2 line as broad as about 1 GHz in a room temperature Cs vapor cell. Then a green laser, the coupling laser at 510.8 nm, further excites a small velocity group of Cs atoms into the Rydberg state $36^2D_{5/2}$ via a sub-Doppler electromagnetically induced transparency (EIT) resonance [10] with a linewidth of approximately 30 MHz. The Cs Rydberg transition $36^2D_{5/2} - 37^2P_{3/2}$ has not been experimentally studied before. To characterize this transition, we accurately measured the frequencies of the probe and the coupling lasers using high resolution wavelength meters (WS7-NIR and 871A-VIS, respectively), determining that the Cs $36^2D_{5/2}$ state is 31308.77 cm^{-1} above the $6^2S_{1/2}$ F = 4 ground hyperfine state. The resonance frequency between $36^2D_{5/2}$ and $37^2P_{3/2}$ states was measured to be 16.316 GHz by RF spectroscopy as given in Fig. 2b with a calibrated signal generator (E8257D).

When a microwave interacts with the Rydberg transition on resonance, atoms in the $36^2D_{5/2}$ state are pumped into the $37^2P_{3/2}$ state, causing a decrease in absorption of the probe laser passing through the vapor cell. The changes in the probe laser light intensity coming out of the vapor cell are detected by a photodetector. In this way, the Rydberg transition functions like a local oscillator for sensitively detecting microwave signals.

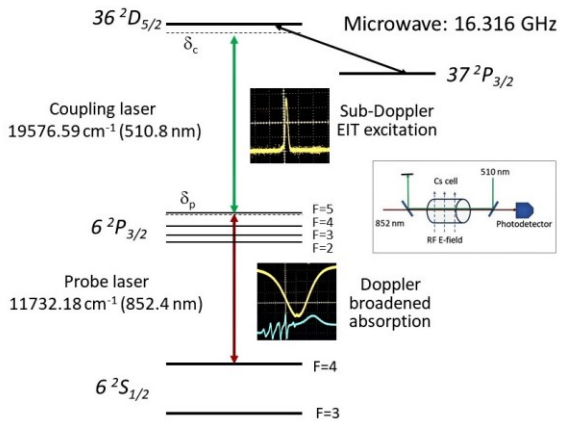

Fig. 1 Atomic transition scheme of the Cs Rydberg oscillator at 16.316 GHz in a room temperature Cs vapor cell. The two laser frequencies were measured using wavelength meters as labeled in the figure. Together with the Doppler-broadened Cs D2 line is the saturated absorption spectrum of the hyperfine transitions between $6^2S_{1/2}$ F = 4 and $6^2P_{3/2}$ F = 2, 3, 4, and 5 states, which serves as the frequency reference. The sub-Doppler EIT spectral line was obtained by sweeping the coupling laser frequency while locking the probe laser frequency to $6^2S_{1/2}$ F = 4 – $6^2P_{3/2}$ F = 5 transition.

III. OSCILLATOR RESPOSES TO MICROWAVE E-FIELD

Fig. 2a presents the observed EIT spectra when relatively strong microwave signals at various powers interact with the Rydberg transition on resonance, causing the EIT spectral line being broadened and split by the Autler-Townes (AT) effect [11]. According to Eq.1, the frequency spacing $\Delta\nu$ of the AT line splitting in Fig. 2a is proportional to the microwave E-field strength E_{MW} [4]. In Fig. 3a, we first plot the measured $\Delta\nu$ as a

function of the E-field strength directly derived from the horn antenna and performed a liner-fit to determine the dipole moment μ_{MW} for the Cs $36^2D_{5/2} - 37^2P_{3/2}$ transition. The linear-fit slope results in $\mu_{MW} = 784$ (ea_0), which is compared in Fig. 4 with the quadratic extrapolation from the known values in [8].

$$\Delta v = \frac{\mu_{MW}}{2\pi\hbar}\frac{\lambda_c}{\lambda_p}E_{MW} \quad (1)$$

where λ_p and λ_c is the probe and coupling laser wavelength, respectively, and $\hbar$ the Planck constant. The $\lambda c/\lambda p$ factor compensates the difference in Doppler effects of the two lasers [4].

More commonly, Eq. 1 is used reversely to derive the absolute E-field strengths from the measured Autler-Townes line splitting spacings when the dipole moment μ_{MW} is known for the Rydberg transition. As $\mu_{MW} = \langle nl|er|n'l'\rangle$ can be theoretically computed from the atomic structure and fundamental constants, the E-field measurements based on Eq. 1 is self-calibrated. Fig. 3b plots the measured E-field strengths (blue squares) as a function of the square-root of the microwave power and compares them with those derived from the antenna (solid line).

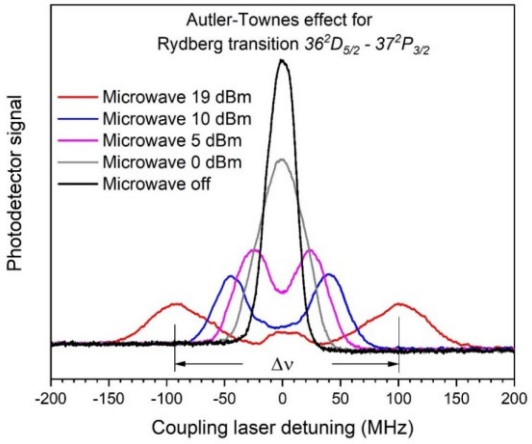

(a)

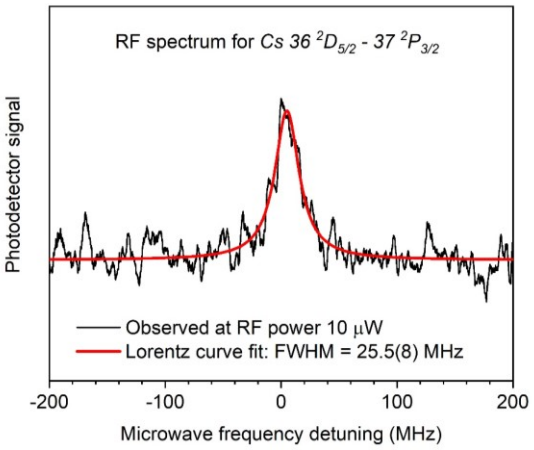

(b)

Fig. 2 a) Observed EIT excitation spectra and Autler-Townes line splitting in strong field regime at various microwave powers; b) Observed RF spectrum in weak E-field regime at E_{MW} = ~1 mV/cm. The line peak measured at ν_0 = 16.316 GHz.

The Autler-Townes method for E-field measurements does not work for weak RF signals when the Autler-Townes effect can be ignored. Fig. 2b above is a RF spectrum, obtained by sweeping the microwave frequency over the Rydberg transition while keeping both laser frequencies fixed, when the microwave power was lowered to 10 μW. In this weak field regime, we measured the resonace frequency of the $36^2D_{5/2} - 37^2P_{3/2}$ transition to be 16.316 GHz with a linewidth (FWHM) of 25.5 MHz. Table 1 summarizes our characterization results of the Cs $36^2D_{5/2} - 37^2P_{3/2}$ transition.

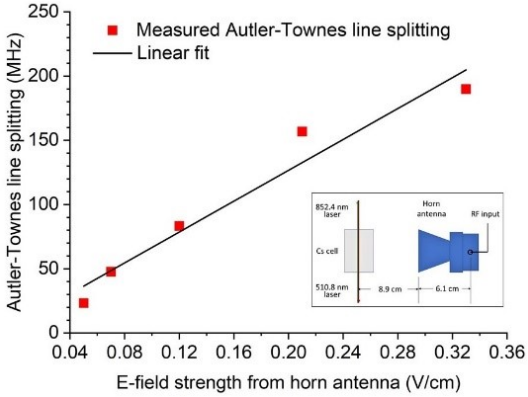

(a)

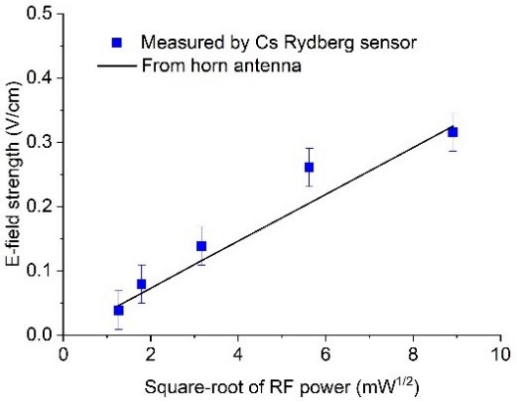

(b)

Fig. 3 (a) Measured frequency spacings of Autler-Townes (AT) line splitting vs. E-field strengths derived from horn antenna. From Eq. 1, the linear fit slope results in a transition dipole moment of μ_{MW} = 784 ea_0. (b) E-field strengths determined from measured frequency spacing Δν of AT line splitting as a funcftion of the square-root of microwave powers. The solid line is the E-field strengths calculated from the antenna.

TABLE I EXPERIMENTAL MEASUREMENT RESULTS OF THE CS RYDBERG TRANSITION OF $36^2D_{5/2} - 37^2P_{3/2}$.

Cs Rydberg state parameters	Measured
Energy of $36^2D_{5/2}$ above ground $6^2S_{1/2}$ F = 4 state	31308.77 cm^{-1}
Resonance frequency of $36^2D_{5/2} - 37^2P_{3/2}$ transition	16.316 GHz
FWHM linewidth	25.5 MHz
Transition Dipole moment	784 ea_0

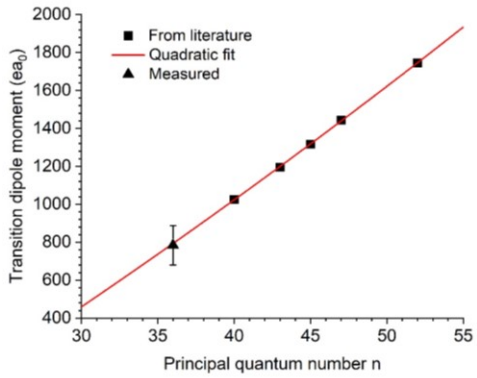

Fig. 4 Measured dipole moment (triangle) of $36^2D_{5/2} - 37^2P_{3/2}$ transition compared with quadratic extrapolation (red line) from known values (squares) of other $n^2D_{5/2} - (n+1)^2P_{3/2}$ transitions in [8].

IV. OSCLLATOR RESPOSES TO AM AND FM MODULATED MICROWAVE E-FIELD

Using the Cs Rydberg transition at 16.316 GHz, we studied the temporal responses of the Rydberg oscillator to amplitude and frequency modulations (AM and FM) of the microwave carrier up to 1 MHz. Fig. 5a and 5b show the Rydberg oscillator's temporal responses when the incident microwave is AM and FM modulated with square waves respectively.

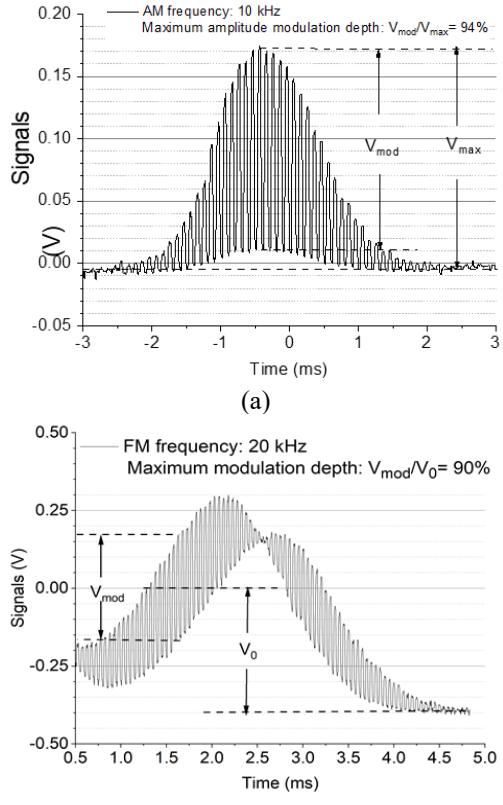

Fig. 5 a) Oscillator temporal response to amplitude modulation of microwave carrier with maximum modulation depth at center frequency of the EIT line; b) Oscillator temporal response to frequency modulation of microwave carrier with maximum modulation depth at side frequency of the Autler-Townes lobe.

The spectra were obtained by slowly sweeping (at 10 Hz) the coupling laser frequency over the EIT resonance while fast modulating the microwave carrier at 10 kHz for AM in Fig. 5a and 20 kHz for FM in Fig. 5b. The horizontal axis in time also represents the frequency detuning of the EIT spectral line. The data reveal that the maximum modulation depth for AM occurs at the center frequency of EIT excitation peak, while the maximum modulation depth for FM is obtained at the side frequency of the Autler-Townes lobes as displayed in Fig. 2a. At low AM and FM frequencies, maximum modulation depths up to 94% were observed. The modulation depths decreased to about 10% as the modulation frequency increased to 1 MHz under current experimental conditions. Fig. 6a and 6b display the oscillator's responses to AM and FM modulated microwaves at 1 MHz, respectively. The output waves at 1 MHz have good signal to noise ratios and are readily to be processed for transmitting digital data through the Rydberg oscillator.

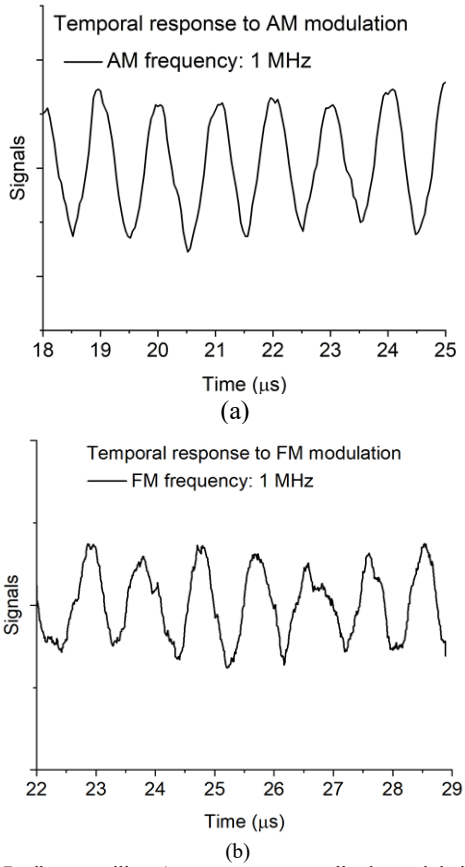

Fig. 6 Cs Rydberg oscillator's responses to amplitude modulation (a) and frequency modulation (b) of microwave carrier E-fields at 1 MHz modulation frequency. The output waves are readily to be processed with a signal re-shaping circuit or algorithm to transmit digital data encoded in the carrier for RF receiver application.

V. SUPERHETERODYNE E-FIELD SENSING

To take advantage of phase sensitive detection, we implemented a superheterodyne [6, 7] E-field sensing scheme as depicted in Fig. 7. A second microwave field as a local

oscillator at frequency ν_{LO} dresses the Rydberg transition and generates a heterodyne wave with the incident RF signal at the difference frequency $\nu_{hetero} = \nu_{Sig} - \nu_{LO}$. The heterodyne signal at ν_{hetero} can then be sensitively recorded using a lock-in amplifier. Fig. 8 presents the lock-in amplifier output of the heterodyne signal as a function of the incident microwave E-field strength. Under current experimental conditions, microwave signals with E-field strength at 10 μV/cm was observed as the signal generator's output power was gradually reduced. This represents a 100-fold improvement in E-field sensing sensitivity compared with not using the heterodyne technique as the RF signal shown in Fig. 2b. The inset in Fig. 8 is an example spectrum of heterodyne signal obtained by the lock-in amplifier at ν_{hetero} = 698 kHz and ν_{LO} = 16.31 GHz (on resonance). The decrease in heterodyne signal intensity for E-field strengths > 0.1 V/cm is attributed to the Autler-Townes effects in the strong field regime as shown in Fig. 2a.

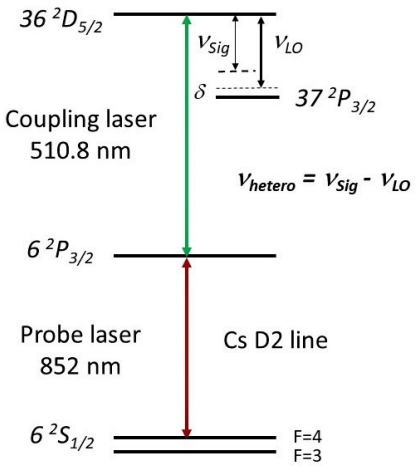

Fig. 7 Atomic transition scheme for superheterodyne E-field sensing. A second microwave field as a local oscillator at frequency ν_{LO} dresses the Rydberg transition and generates a heterodyne wave at difference frequency ν_{hetero} with the incident RF signal. The heterodyne signal at ν_{hetero} is sensitively detected using a lock-in amplifier.

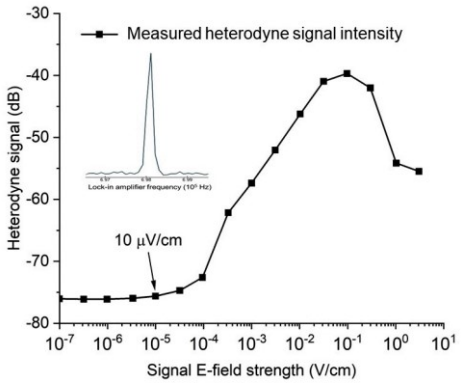

Fig. 8 Observed heterodyne signal intensity as a function of the microwave E-field strength with the local oscillator frequency on resonance at ν_{LO} = 16.31 GHz. Electric field at 10 μV/cm was observed with superheterodyne detection, a 100-fold improvement in sensing sensitivity compared with not using the superheterodyne technique. The inset is an example heterodyne spectrum obtained by the lock-in amplifier at ν_{hetero} = 698 kHz.

The superheterodyne detection technique is so sensitive that incident microwave signals at frequencies off-resonance from the Rydberg transition can still be detected by the oscillator. Fig. 9 plots the spectra of the heterodyne signals as a function of the incident microwave frequency with the local oscillator synchronized at a fixed ν_{hetero} = 10 kHz. The result reveals a continuous sensing range about 5 GHz around the Rydberg transition at 16.31 GHz. Such continuous-frequency sensing can be extended to the entire radio frequency spectrum as modeled in Fig. 10.

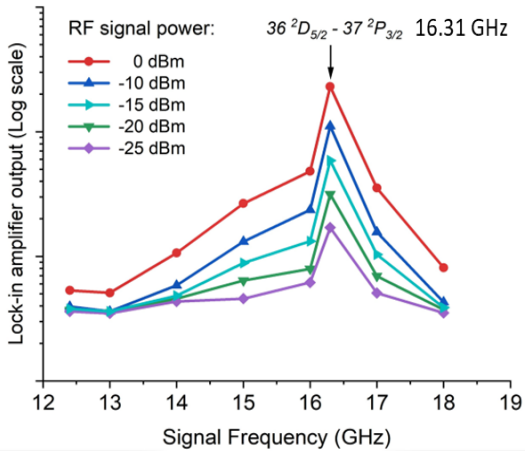

Fig. 9 Recorded heterodyne signal intensity as a function of the incident microwave signal frequency. In this measurement, the local oscillator was synchronized with the signal at a fixed ν_{hetero} = 10 kHz. The result shows a continuous sensing range of about 5 GHz around the Rydberg transition.

VI. DISCUSSIONS

A. Cs Rydberg transition frequencies

Cs Rydberg atoms have accessible Rydberg transitions at frequencies ranging from MHz all the way to THz covering all radio frequency (RF) bands for various applications. In addition to the $36^2D_{5/2} - 37^2P_{3/2}$ transition studied in this work, we have modeled and computed the Cs Rydberg transition frequencies for six dipole-allowed transition series using Eq. 2 as a function of the principal quantum number n of the initial state of the Rydberg transitions.

$$\nu_{MW} = \frac{R_{yCs}}{h}\left(\frac{1}{(n-\delta_{nlj})^2} - \frac{1}{(n'-\delta_{n'l'j'})^2}\right) \quad (2)$$

where R_{yCs} is the Rydberg constant for Cs, h the Planck constant. n and n′ are the principal quantum number of the initial and final state respectively, and δ_{nlj} and $\delta_{n'l'j'}$ are the corresponding quantum defects of the two states. The numerical values of R_{yCs} and δ_{nlj} given in [1] are used for the calculation. To directly relate the Rydberg transition frequency to the coupling laser excitation as depicted in Fig. 1, we plot the computed Rydberg transition frequency (labeled as microwave frequency) as a function of the coupling laser wavelength in Fig. 10.

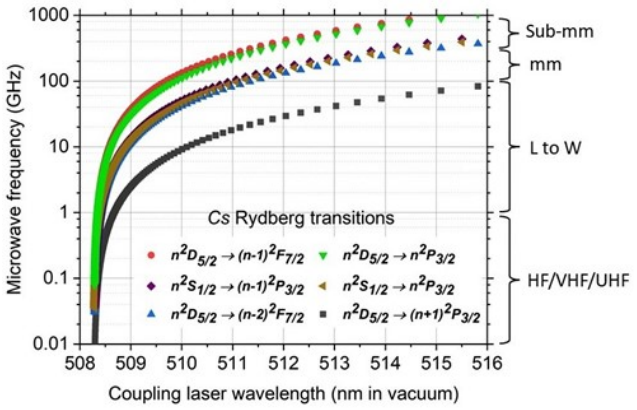

Fig. 10 Computed Cs Rydberg transition frequencies of six dipole-allowed transition series as a function of the coupling laser wavelength. The vertical axis is in log scale and the corresponding microwave bands are labeled next to the right vertical axis.

In Fig. 10, the shorter laser wavelengths correspond to Rydberg states at higher n, while the longer wavelengths are for Rydberg states at lower n. Using the $n^2D_{5/2} - (n+1)^2P_{3/2}$ transitions as examples, a microwave oscillator at 30 MHz can be realized at n = 275 with the coupling laser wavelength tuned to λ = 508.316 nm. While for a microwave frequency at 71.7 GHz, we have n = 23 and λ = 515.09 nm. In the figure, we also label the corresponding microwave bands next to the right vertical axis.

B. Transition from strong field regime to weak field regime

In Fig. 2a and 2b, we showed the Rydberg oscillator's responses to the interacting microwaves at various signal power levels. With relatively strong signals (in the strong field regime), the Autler-Townes effect causes a decrease at the EIT line center that splits the spectral line as in Fig. 2a. While, when the oscillator responds to a weak microwave signal (in the weak field regime), the Autler-Townes effect is diminished, and the incident microwave instead increases the EIT line intensity as in Fig. 2b. The RF spectra obtained at various microwave power levels displayed in Fig. 11 clearly show the transition from the strong field regime to the weak field regime. Specifically, a decrease signal was observed at resonance frequency for RF powers $\geq$ 0 dBm, while an increase signal was obtained for RF powers $\leq$ -5 dBm under our experimental conditions. The transition occurs between 0 dBm and -5 dBm, corresponding to E-field strengths between 0.04 V/cm and 0.02 V/cm, respectively.

VII. CONCLUSIONS

We implemented and characterized a Cs Rydberg atomic oscillator using the $36^2D_{5/2} - 37^2P_{3/2}$ transition in Ku band at 16.316 GHz for continuous and time-varying microwave E-field sensing. The energies and the transition dipole moment of the Cs $36^2D_{5/2} - 37^2P_{3/2}$ system were experimentally measured for the first time. In addition, we also realized amplitude and frequency modulations of the Cs Rydberg oscillator at rates up to 1 MHz for data transmission application. To enhance the oscillator's response to weak signals, we incorporated the superheterodyne technique into the Rydberg oscillator system and observed microwave signals at E-field strength of 10 μV/cm, a 100-fold improvement in oscillator's sensitivity compared with not using the superheterodyne method. Finally, our modeling and computation show that a Cs Rydberg atomic oscillator can be tuned to a broad range of frequencies from below L band all the way to mm-waves for various RF applications.

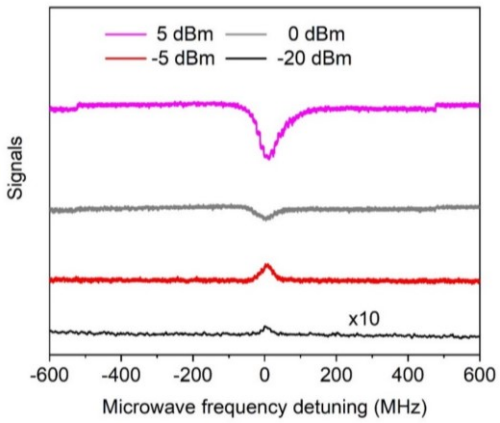

Fig. 11 RF spectra at various signal generator powers. In the strong field regime, a decrease signal was observed for RF powers $\geq$ 0 dBm, while an increase signal was obtained for RF powers $\leq$ -5 dBm. The transition occurs between 0 dBm and -5 dBm, corresponding to E-field strengths between 0.04 V/cm and 0.02 V/cm, respectively.

REFERENCES

[1] T. F. Gallagher, *Rydberg Atoms*, Cambridge University Press 1994.

[2] J. A. Sedlacek, *et al*., *Atom-based vector microwave electrometry using rubidium Rydberg atoms in a vapor cell*, Phys. Rev. Lett 111, 063001(2013).

[3] H. Fan et al., *Atom based RF electric field sensing*, J. Phys. B: At. Mol. Opt. Phys, 48, 202001(2015).

[4] C. L. Holloway et al., *Atom-based RF electric field metrology: from self-calibrated measurements to subwavelength and near field imaging*, IEEE Trans Electromagnetic Comp. 59, 717(2017).

[5] D. H. Meyer et al., *Digital communication with Rydberg atoms and amplitude-modulated microwave fields*, App. Phys. Lett. 112, 211108 (2018).

[6] M. Jing et al., *Atomic superheterodyne receiver based on microwave-dressed Rydberg spectroscopy*, Nature Physics 16, 911–915 (2020).

[7] D. H. Meyer *et al*., *Waveguide-coupled Rydberg spectrum analyzer from 0 to 20 GHz*, Phys. Rev. Appl. 15, 014053*(2021)*.

[8] M. T. Simons, J. A. Gordon, and C. L. Holloway, *Simultaneous use of Cs and Rb Rydberg atoms for dipole moment assessment and RF electric field measurements via electromagnetically induced transparency*, J. Appl. Phys. 120, 123103(2016).

[9] D A Anderson, R. E. Sapiro, and G. Raithel, *A Self-Calibrated SI-Traceable Rydberg Atom-Based Radio Frequency Electric Field Probe and Measurement Instrument*, IEEE Trans. Antennas and Propagation 69, 5931(2021).

[10] K. –J. Boller, A. Imamoglu, and S. E. Harris, *Observation of electromagnetically induced transparency*, Phys. Rev. Lett. 66, 2593-2596(1991).

[11] L. Giner et al., *Experimental investigation of the transition between Autler-Townes splitting and electromagnetically-induced transparency models*, Phys. Rev. A 87, 013823(2013)